AIAA Modeling and Simulation Technologies Conference and Exhibit
21 - 24 August 2006, Keystone, Colorado

AIAA 2006-6261

Development of Small Unmanned Aerial Vehicle Research Platform: Modeling and Simulating with Flight Test Validation

Captain Nidal M. Jodeh* and Major Paul A. Blue†
Air Force Institute of Technology, Wright Patterson AFB, OH, 45433

Second Lieutenant Athon A Waldron‡
Air Force Institute of Technology, Wright Patterson AFB, OH, 45433

This paper describes the development of a small unmanned aerial vehicle aerodynamic model and six degree of freedom simulation for a flight test platform. The aircraft, a SIG Rascal 110 radio controlled (R/C) aircraft equipped with a Piccolo II Autopilot Controller, will primarily be used for advanced navigation, guidance, and control research by the Advanced Navigation Technology Center at the Air Force Institute of Technology. The research platform was developed in a two part approach. Part one began with assembly, modifications, physical measurement, and modeling of the aircraft, to include experimental determination of the airfoil, inertia, and center of gravity information. Aircraft modeling employed the US Air Force Digital Datcom. Part two included development of a Matlab/SIMULINK six degree of freedom (6-DoF) simulation. A build up of the physical measurements, aerodynamic stability and control derivatives, forces and moments, and equations of motion comprise the 6-DoF simulation. Part two also completed the set up of the hardware in the loop simulation, provided by the autopilot manufacturer. Longitudinal open loop flight test maneuvers were performed and compared in both the Matlab/SIMULINK and hardware in the loop simulations. The same maneuvers were performed in flight test to validate the simulation. Using actual control surface telemetry, the simulation model received the same commands transmitted to the flight test vehicle. Telemetry collected from simulations was plotted and compared against telemetry from flight test.

I. Introduction

A. Motivation

The Department of Defense drive towards using autonomous Unmanned Aerial Vehicles (UAVs) of all sizes, and the visions of using them for almost any task leads the way for a more effective force that can operate more efficiently (less costly with fewer operators). UAVs have exploded in popularity among the aviation research communities, both in the civilian and military sectors. The small UAV, in particular, is relatively inexpensive when compared to a large scale UAV such as the US Air Force (USAF) Predator or the US Army's Shadow. The small UAV offers a multitude of autonomous flight research applications that once seemed out of reach, including autonomous formation flight, collision avoidance, sensors platform, and advanced navigation studies.

In general, modeling, simulating, and flight-testing of full scale aircraft is well documented. However, literature becomes less available when it comes to small UAVs. Few relevant articles discussing the detailed modeling, stability, and simulation development of small UAVs were found. In 2003, Ref. 1 conducted research similar to the work presented here[0], but used full scale aircraft wind tunnel data to build an aerodynamic model. In 2004, a hardware-in-the-loop simulation and a small UAV model to demonstrate distributed coordination and control of a multi-UAV test bed.[2] In 2001, experiments with simulation to compliment low-cost UAVs were conducted.[3] All the

* Aeronautical Engineer, Air Force Research Labs, Air Vehicles Directorate, Professional Member.
† Instructor of Aerospace Engineering, Air Force Institute of Technology, Professional Member.
‡ Civil Engineer, US Air Force, Professional Member

aforementioned references conducted similar work, but do not address the specific needs of modeling and simulating small UAVs

A literature review reveals there are no specific standards for small autonomous UAV handling qualities. Current standards for handling qualities apply only to piloted aircraft. Without the pilot in the loop, the envelope for handling qualities surely expands, becoming less restrictive. Although handling qualities is not a direct goal of this paper, this research directly contributes to handling qualities determination. Reference 4 also found a lack of relevant articles on the subject of UAV stability and handling qualities. "No direct relevant articles discussing dynamic stability and handling qualities for small UAVs."[4]

The research community does not clearly define the term small UAV. Reference 4 defines a small UAV as one with a wingspan approximately 1.64 to 4.92 feet for purposes of their research. A Micro Air Vehicle (MAV) with a two foot wingspan is considered small.[5] Others characterize a small UAV as one with a nine foot wingspan.[6] The 2002 Unmanned Aerial Vehicles Roadmap, from the Office of the Secretary of Defense, states that small UAVs are those having a Reynolds number less than 1 million.[7] The aircraft chosen for this research meets the Roadmap criteria for Reynolds number, shown later. For purposes of this research, UAVs with wingspans of 10 or fewer feet are considered small. For the remainder of the research, the term "small" UAV is implied.

B. Problem Statement

Little data is available on the SIG Rascal 110 for modeling and simulation. The challenges are to accurately model the existing airframe, develop a high fidelity simulation to run the model, and validate the simulation with flight test data.

C. Methodology

In order to tackle the problem statement, an accurate physical, inertial, and aerodynamic model of the Rascal 110 for use in simulation must be developed first. Incorporating classical airframe analysis as well as more modern techniques improves the model's fidelity. Next, create a Matlab/SIMULINK simulation of the aircraft using the model developed. This simulation will represent the aircraft's open loop flight characteristics. Also incorporate the Rascal 110 model into a commercial Hardware in the Loop (HITL) simulation provided by the autopilot manufacturer. This particular simulation seeks to represent the aircraft's closed loop flight characteristics for use in test team training and bench testing flight tests. Finally, characterize the performance of the UAV through flight tests and to collect open flight data that can be used to validate the simulations.

D. Significance of Research

While the Rascal 110 is widely used as a research platform, no aerodynamic data existed. Therefore, the aerodynamic model and simulation developed in this research will contribute to the UAV research community as a whole. Furthermore, future researchers will be able to apply the methods presented to develop aerodynamic models and simulations for any small UAV.

E. Preview

Section II introduces the equipment used and provides some background on open loop flight-testing. Section III methodically steps through complete collection and development of the physical, inertial, and aerodynamic characteristics of the aircraft. Section IV covers the development use of the Matlab/SIMULINK and Hardware in the loop simulations. Section V then compares results from the Matlab/SIMULINK simulation to the open loop flight tests and the HITL simulation.

II. Background

The aircraft chosen as the research platform was the Rascal 110 R/C aircraft constructed by the SIG Manufacturing Company, Inc. Stability, performance, weight, and balance data was not available from SIG and had to be determined during the course of this research. The aircraft is a high wing, tail wheel configured aircraft. The aircraft is powered by the FS-120S III four-cycle engine by O.S. Engines and fitted with a 16 x 8 propeller from APC. Combined, the engine and propeller weighed 32.5 ounces, and was capable of pulling the SIG Rascal 110 over 60 knots on a calm day. The Radio Control (R/C) system is a Futaba 9CAP/9CAF 8 Channel transmitter with a Futaba R149DP PCM 1024 receiver. High torque servos from Futaba actuated the control surfaces. The autopilot system, acquired from Cloud Cap Technologies, includes the airborne avionics, Ground Station Interface, manual control box, hardware in the loop simulator, and software. The airborne component, the Piccolo II, is a fully autonomous autopilot system for small-unmanned aircraft. Before fully autonomous flights were scheduled, the

Piccolo II was used to collect flight data and transmit telemetry. A list of available telemetry is given in the Appendix, Table 16.

Autopilot controllers use feedback control loops to maintain desired parameters. With the control loops turned off, the autopilot has no information about the aircraft's current state. Thus, when the control surfaces receive commands, the aircraft behaves in an open loop condition, meaning the response to the command is purely the aircraft's natural response.

Open loop flight test seeks to capture the natural system response to prescribed control inputs. Flight tests without feedback control can reveal the natural response of the aircraft at different airspeeds, altitudes, and configurations. Thus allowing autopilot designers to better tailor controllers to suit the aircraft.

III. Development of UAV Aerodynamic Model

The aircraft employs a high-wing semi elliptical planform. The term 'semi-elliptical' is used since the trailing edge of the wing resembles that of an elliptical wing, but has a straight leading edge, Fig 1. The manufacturer provided some dimensions; wing span (b), wing area (S), and airfoil type.[8] All the remaining dimensions were determined by physically measuring the aircraft.

A. Physical Geometry

The mass of the aircraft was determined by placing three digital scales under each of the three landing gear wheels. The aircraft was configured with the engine, propeller, empty fuel tank, five servos, R/C receiver, Piccolo II, Fail Safe Control Relay, and 14-AA Nickel Metal-Hydride (NiMH) batteries. Table (1) lists the component weights.

Root chord measurements for the vertical and horizontal tails included the respective control surfaces. Table (2) lists the mass properties and dimensions of the Rascal 110. Aspect Ratio (AR) was calculated using AR = b2/S, the aspect ratio equation for a non-rectangular wing, resulting in AR = 7.94.

The wing, vertical tail, and horizontal tail planforms are analyzed next. The model input into the simulators, developed in the next Section, use a theoretical rectangular wing, vertical and horizontal tail shape. More specifically, the aerodynamic math modeling software, discussed later, can treat a straight-tapered or non-straight tapered wing, but not elliptical. The rectangular planform simplifies the modeling of the aircraft, due to its linear nature. Additionally, since the manufacture and use of elliptical planforms is nearly non-existent, literature on modeling such wings is also nearly non-existent. By using the earlier values for span, root chord, area, and Eqs. (1) and (2), the chord length at the tip of the theoretical rectangular wing can be calculated. By first solving for the taper ratio (λ), the ratio of the tip to root chord, the tip chord can be determined. The horizontal stabilizer and elevator also shared a semi-elliptical planform, although slightly more distorted along the trailing edge to accommodate the rudder deflection. The results are given in Table (3).

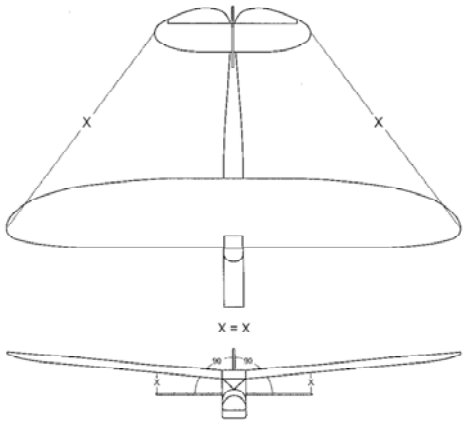

Figure 1. SIG Rascal 110 Top and Front Views[8]

Table 1. Component Weights

Component	Weight (lbf)
Aircraft (Empty Tank, 5 Servos, Engine, Receiver)	14.19
Piccolo II with 10-AA NiMH Battery Pack	1.2
Fail Safe Control Relay	.1
4-AA NiMH Servo Battery Pack	.25
50 oz of Nitromethane fuel	3.0
Gross Take Off Weight	18.74

Table 2. Rascal Physical Dimensions

NAME	SYMBOL	VALUE
Wing Reference Area[8]	S_W	10.56 ft^2
Wing Span[8]	b_W	9.16 ft
Aspect Ratio	AR	7.94 ft
Wing Root Chord	c_{RW}	1.33 ft
Horizontal Tail Area	S_H	1.99 ft^2
Horiz. Tail Span	b_H	3.04 ft
Horiz. Tail Root Chord	c_{RH}	0.833 ft
Vertical Tail Area	S_V	0.773 ft^2
Vert. Tail Span	b_V	0.937 ft
Vert. Tail Root Chord	c_{RV}	1.0833 ft
Aircraft Mass (Empty)	M	0.4895 Slugs

$$S = \frac{c_{RW}(1+\lambda)}{2} b \tag{1}$$

$$\lambda = \frac{c_{RW}}{c_{TW}} \tag{2}$$

Table 3. Planform Taper Ratios and Tip Chord Lengths

Term Name	Symbol	Value
Wing Taper Ratio	λ_W	0.7295
Wing Theoretical Tip Chord	c_{TW}	0.9697 ft
Horiz. Tail Taper Ratio	λ_H	0.5708
Horiz. Tail Theoretical Tip Chord	c_{TH}	0.8336 ft
Vertical Tail Taper Ratio	λ_V	0.5708
Vert. Tail Theoretical Tip Chord	c_{TV}	0.6184 ft

Other key characteristics of the wing, vertical tail, and horizontal tail include dihedral (Γ), incidence angle (i), twist, leading edge sweep (ΛLE), and quarter chord sweep (Λc/4). An inclinometer was placed centered and perpendicular to the chord direction and at one half the distance from the wing root chord to the wing tip. The horizontal and vertical tails have no dihedral. The vertical tail was determined to have a leading edge sweep of 25 degrees. The quarter chord was assumed not to be swept for purposes of modeling, and therefore the trailing edge is forward swept to accommodate the taper ratio and tip chord. Table (4) shows the values for incidence, dihedral, sweep, and twist.

Table 4. Rascal Incidence, Dihedral, Twist, and Sweep

Term	Symbol	Wing (deg)	Horizontal Tail (deg)	Vertical Tail (deg)
Incidence	i	2 deg	2 deg	0 deg
Dihedral	Γ	2 deg	0 deg	0 deg
Twist	-	0 deg	0 deg	0 deg
Leading Edge Sweep	Λ_{LE}	0 deg	0 deg	25 deg
Quarter Chord Sweep	$\Lambda_{c/4}$	0 deg	0 deg	0 deg

To model the fuselage, a reference plane was defined from the center of the propeller to the end of the fuselage and parallel to the ground (with the aircraft in a level flight orientation). The fuselage was then sliced at regular intervals, called Stations, and the cross sectional area was determined with respect to the distance from the front of the cowling (X) and the distance above (Z_U) and below (Z_L) the reference plane. Table (5) lists the meanings of each dimension. Figure (15) provides a visual representation and Table (17) lists the measured dimensions of the Rascal 110, both in the Appendix.

Table 5. Cross Sectional Area Dimension Definitions

Designation	Meaning
Station Number	Designation of Cross Section Location
X (ft)	Distance Back From Front of Engine Cowling
S (ft^2)	Cross Sectional Area of Station Number
Z_U (ft)	Coordinate Distance Above Reference Plane
Z_L (ft)	Coordinate Distance Below Reference Plane

B. Products of Inertia

Product of inertia values for the SIG Rascal were required for simulation. Experimental inertia data was obtained by physically hanging the aircraft and swinging it with constant oscillations. This method was chosen since it generated more accurate results using the actual flight test vehicle.

The aircraft hung from a single point, allowing the CG to fall directly below the hanging point, like a plumb bob. The aircraft was free to swing in the XY, XZ, and YZ planes. A swinging gear (i.e. a wire harness) was constructed to hang the aircraft. Figure (2) shows the Rascal in the vertical orientation; from here it was swung in the XY and XZ planes. Figure (3) is a schematic of Fig. (2). Since the CG lay inline with the hanging wire, a laser-line was projected on to the body and aligned with the wire. The laser-line now passed through the CG. A secondary result of this procedure revealed the location of the CG along the Z-axis when the laser-line was projected down the side of the fuselage.

Figure 2. Aircraft set up for Inertia Swings

Using an inclinometer placed in the corner where the wing trailing edge meets the fuselage, the aircraft was displaced 10 degrees from its resting position along the XY plane. It was then released and allowed to oscillate freely in the XY plane. Ten oscillations were counted and timed. These first ten cycles allowed the aircraft to settle into a natural and repetitive rhythm, minimizing effects of the first oscillation due to the initial release. The aircraft was allowed to continue swinging until the oscillations completely dampened out; again total oscillations were counted and timed where the time final is T_f. The procedure was repeated three times in each plane. For the XZ plane, the aircraft was oriented parallel to the ground. In the XZ plane, the aircraft was only displaced 5 degrees as it provided a less aggressive arc, but sufficient results. Table (6) list the average results of each swing.

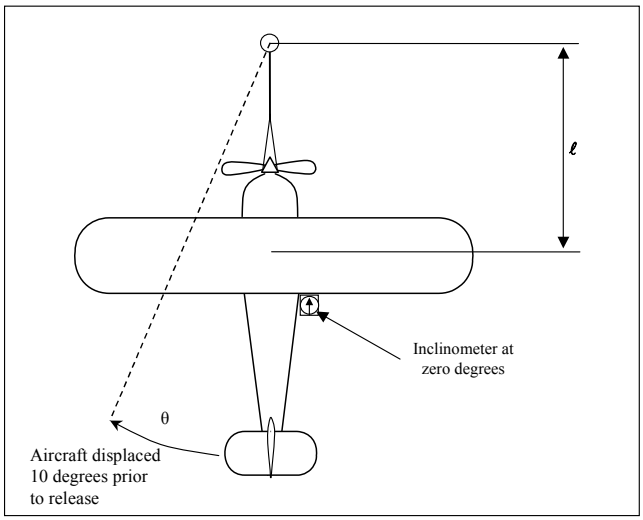

Figure 3. Schematic of Aircraft Set up for Inertia Swing

Table 6. Inertia Test – Displacement in Each Plane

3 Run Avg	Displacement (deg)	Ref. Length ℓ_{CG} (ft)	Time for 10 Oscillations (Sec)	Time to Damp Out T_f (min:sec)	Avg Time Per Oscillation T_1 (sec)
YZ Plane	5	3.125	23.23	No Data	2.323
XZ Plane	10	2.67	21.76	1:24	2.176
XY Plane	10	2.67	22.52	2:28	2.253

The raw data from the inertia swing tests was placed through a series of equations to determine the inertia values. The data reduction method for calculating product of inertia for a swinging aircraft requires mass of the vehicle and swinging apparatus, the length from the point of oscillation to the CG of the aircraft, and the time to swing through one oscillation.[9] The procedures for calculating the product of inertia are based on the equation of motion for a simple pendulum, about a fixed pivot point above the CG.[9] The equations for a simple pendulum are manipulated to solve for product of inertia and applied here. Calculate the damped natural frequency (ω_d) next by Eq. (3)[9], where T_1 is the average time per oscillation in each axis.

$$\omega_d = \frac{2\pi}{T_{1X}} \tag{3}$$

Since the oscillations were considered damped, the natural, undamped frequency is determined next. In order to extract the undamped frequency of oscillation, the real ($\mathcal{Re}$) and imaginary ($\mathcal{Im}$) portions of the damped oscillations must be calculated. The undamped natural frequency lies on the imaginary plane with real and imaginary components. The damped natural frequency, ω_d, is equal to $\mathcal{Im}$ portion of the undamped natural frequency and lies on the imaginary axis. The oscillations decay exponentially by Eq. (4).

$$e^{-\mathcal{Re}t} = e^{-t/\tau} \tag{4}$$

where, $\tau = 1/\mathcal{Re}$ is the time constant, and noting that $e^{-5} \approx 0$, or where, $t = T_f = 5\tau$, the oscillation has essentially died out. Now, $T_f = 5\tau = 5/\mathcal{Re}$, or by Eq. (5).

$$\mathcal{Re} = 5/T_f \tag{5}$$

Based on the geometry of the imaginary plane and the location of the undamped natural frequency, ω_n can be determined by Eq. (6).

$$\omega_n = \sqrt{\mathcal{Re}^2 + \mathcal{Im}^2} \tag{6}$$

"The moment of inertia of the airplane about an axis through its center of gravity equals the moment of inertia of the entire pendulum about the axis of oscillation minus the moment of inertia of the swinging gear about the same axis minus the additional moment of inertia due to the displacement of the center of gravity of the airplane from the axis of oscillation."[9] Since the swinging gear has negligible mass compared to the aircraft, it will be ignored. Using gravity (g) equal to 32.174 ft/sec^2 and the mass (M) of the vehicle equal to 0.489519 slugs, Eq. (7) yields product of inertia for either the damped or undamped natural frequencies. The first term considers the entire swinging apparatus set up, including the aircraft and displaced CG. The second term, subtracted from the first, corrects for displaced GG.[9]

$$I_{XX} = M\ell_{CG}\left(\frac{1}{\omega}\right)^2 g - M\ell_{CG}{}^2 \tag{7}$$

The resulting undamped natural frequencies and respective product of inertias for each plane are collected in Tables (7) and (8). Product of inertia in the I_{XZ} is considered zero since the aircraft is symmetric about that plane. The inertia values are calculated using the undamped frequency.

Table 7. Undamped Frequencies of Oscillation

Axis of Oscillation	Undamped Frequency ω_n (sec)
X	2.7051
Y	2.8881
Z	2.7892

Table 8. Undamped Products of Inertia

Axis of Oscillation	Undamped Inertia (slugs·ft^2)
X	I_{XX} = 1.9456
Y	I_{YY} = 1.5505
Z	I_{ZZ} = 1.9147
-	I_{XZ} = 0

C. Center of Gravity Determination

For the Center of Gravity (GC) along the Y and X axis the aircraft was set upon three identical digital scales, one under each wheel. The tail wheel scale was raised eight inches in order to put the aircraft in a level flight configuration. An inclinometer was centered on wing root chord and aligned parallel with the X axis. The tail was raised until the inclinometer read zero. This method for level flight was used as reference for all level flight lab measurements. The scales under the left and right main gear read 6.845 and 6.801 lbf respectively. The tail wheel scale reported 1.9841 lbf. A force and moment balance procedure indicated the CG along the x-axis was 21 inches back from the front of the cowling. For ease of calculations, the CG along the y-axis was assumed to be at the center. These two positions were temporarily marked on the fuselage. When the aircraft was hung for the moment of inertia swing, a laser line was projected along the body to aid in finding the z-axis location of the CG. The previous sub-section, described how the z-axis was determined. Figure (4) shows where the CG of the Rascal was found.

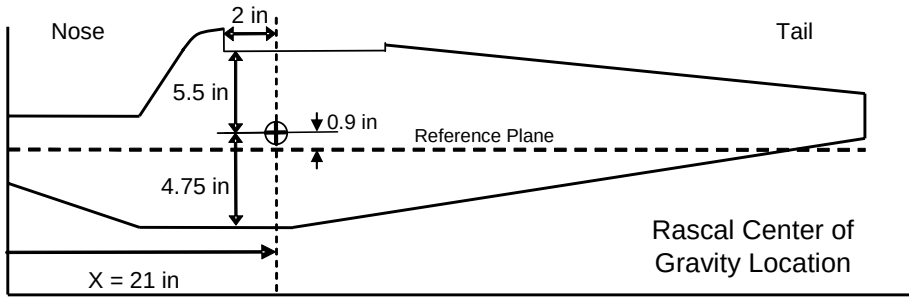

Figure 4. Rascal UAV Center of Gravity Location

D. Airfoil Analysis

The Rascal's wing employs an airfoil that is the sum of two airfoil designs joined at the chord lines, an Eppler 193 (E193) upper half and an Eppler 205 (E205) lower half. Wind tunnel data existed for both airfoils separately, but not in the joined configuration.

For accurate simulation, a wing model is required; specifically three values as a function of the wing angle of attack; the lift coefficient (*Cl*), drag coefficient (*Cd*) and coefficient of moment (*Cm*) are required. The notation of *Cl*, *Cd*, and *Cm* use lower case letters to denote a two-dimensional infinite wing analysis. For an actual finite three-dimensional wing, the terms *Cl*, *Cd*, and *Cm* are modified with capital letters; for example C_L, C_D, and C_M.[10]

Airfoil data was provided as a function of Reynolds-number.[§] Using an average wing chord of 1.25 ft, and a velocity of 67.51 ft/sec at an altitude of 1000 ft above sea level, the Reynolds-number (*Re*) was found to be 523,588.

[§] All airfoil data was derived from Nihon University Aero Student Group (NASG) website. http://www.nasg.com/afdb/index-e.phtml

The highest two Reynolds-numbers available from airfoil databases were chosen for the E193, Re = 303,100 and Re = 204,200, and for the E205, Reynolds-number = 304,300.

The NASG Database revealed that the E205 and E193 airfoils were similar in shape and properties. The E193 has a slightly smaller trailing edge thickness below the chord line and behind the point of maximum thickness as compared to the Rascal airfoil. The E205 is thinner above the chord line and behind the point of maximum thickness.

Further investigation into the lift curves show the E205 has a slightly higher coefficient of lift per degree of angle of attack, alpha, Fig (5). However, the rate of lift per degree of alpha, or the slope of the curves, is the same. Additionally, the E193 lift-curve slopes at the highest and second highest available Reynolds-numbers proved to be nearly identical except for the range of measured data.

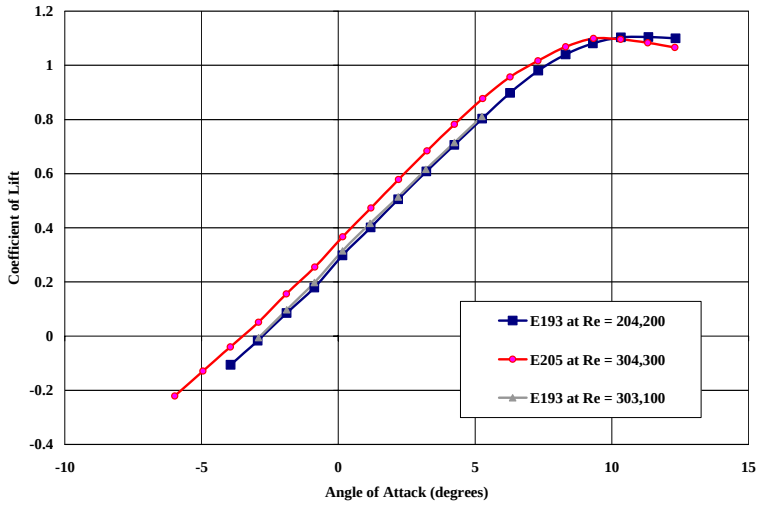

Figure 5. Lift Curve Slopes of E193 and E205

Because it shares the same upper surface, the E193 at a Reynolds-number of 204,200 was ultimately chosen as the airfoil for simulation. The data for the E193 at the Reynolds-number of 204,200 is presented.

The data for the coefficient of drag provided is assumed to be the drag coefficient when the lift is zero, also known as the parasite drag (Cd_o). Since total drag requires the wing aspect ratio and span efficiency factor, it is reasonable to assume the drag provided by the NASG Database is not total drag. To find total drag, parasitic drag must be added to induced drag (Cd_i). The total wing drag (Cd), is the parasite drag plus the induced drag, as shown in Eq. (8).[10] The induced drag, Eq. (9), is a function of aspect ratio, lift coefficient, and span efficiency.[10] The span efficiency factor is 0.7 for a rectangular wing, and 1.0 for a true elliptical wing.[10] Since the model represented in the simulation incorporates a rectangular wing, 0.7 was chosen as the span efficiency factor. The Aspect Ratio of 7.94 and (Cl) from -0.106 to 1.1 were used.

$$Cd = Cd_i + Cd_o \tag{8}$$

$$Cd_i = \frac{Cl^2}{\pi \cdot AR \cdot e} \tag{9}$$

The Matlab simulation developed requires stability and control derivatives. The US Air Force Stability and Control Digital Datcom software, to be discussed later, outputs the required derivatives. Airfoil data input to Digital Datcom must comply with the National Advisory Committee for Aeronautics (NACA) designation. After establishing a common coordinate system and calculating the amount of camber per chord, position of maximum camber as a percentage of chord, and the maximum thickness in percentage of chord, the E193 airfoil can be represented by a NACA equivalent. Using airfoil information from the NASG Database, the NACA equivalent was found to be 4310.

E. Engine and Propeller Model

A linear look up table represented the engine model; revolutions per minute by power in watts. Although a more accurate curve with torque is preferred, engine performance data was not available. The propeller model consists of four variables. The coefficient of thrust (C_t), coefficient of power (C_p), and efficiency in percent are all functions of the Advance Ratio (J). The propeller model was developed using software provide by Cloud Cap Technologies.** Three parameters needed to fully describe the propeller geometric profile. Chord length and pitch angle twist as a function of the propeller radius must be known and an airfoil data file similar to the wing data file is needed. The Rascal 110 was equipped with a 16x8 propeller from APC. Table (9) lists the estimated 16x8 propeller performance data.

Table 9. Estimated 16x8 Propeller Performance Data at 5000 RPMs

J	C_P	C_t	%
0.000	0.023	0.073	0.000
0.010	0.023	0.072	0.031
0.020	0.024	0.071	0.061
0.030	0.024	0.071	0.090
0.040	0.024	0.070	0.118
0.050	0.024	0.070	0.146
0.060	0.024	0.069	0.173
0.070	0.024	0.068	0.199

F. US Air Force Stability and Control Datcom

The Stability and Control Data Compendium, Datcom for short, provides a "systematic summary of methods for estimating basic stability and control derivatives."[11] The Datcom is over 1500 pages of detailed methodology to determine stability and control characteristics of a wide variety of aircraft and aircraft configurations. "For any given flight condition and configuration the complete set of derivatives can be determined without resort to outside information."[11] Primarily intended for preliminary use, ahead of test data, it is designed to give an initial look at the stability performance of an aircraft design. However, it is not intended to be used in lieu of wind tunnel or flight test data. In 1979, the Datcom was re-written in FORTRAN IV computer language. Re-named the USAF Stability and Control Digital Datcom, it became an efficient, user-oriented computer program.[11]

G. Datcom Inputs

Inputs to Datcom include desired flight conditions, aircraft attitudes, physical geometry, and desired outputs. Datcom treats inputs that represent a traditional wing-body-tail configuration and any control or high lift devices.[11] Some non-standard geometries can be treated as well. Datcom inputs were assumed for a straight-tapered or non-straight-tapered wing, which is why the theoretical rectangular wing was devised in an earlier section. For the longitudinal characteristics, the program assumes a mid-wing configuration. The Rascal uses a high-wing configuration, and this introduces a potential source of error. A brief list of input is found in Table (10).

Table 10. Inputs to Digital Datcom; A Brief List

Input	Symbol	Value	Comments
Mach	M	.061	Actual Flight Test Mach
Angle of Attack	A	-10 to 28 deg	Varied Range By 2 deg Increments
Altitude	Alt	1000 ft	Above Sea Level, Actual Flight Altitude
Weight	W	15.74 lbf	Measured, Empty Weight, Flight Configuration
Reference Area	S_{REF}	10.56 ft^2	Measured Wing Area
Reference Chord	$\bar{c}_{REF}$	1.25 ft	Measured Average Chord Length
Reference Span	b_{REF}	9.16 ft	Measured Wing Span
A/C x-axis CG	x_{CG}	2 ft	Measured Back From Front of Cowling
A/C z-axis CG	z_{CG}	0.08 ft	Measured up from Fuselage Reference Line
Wing and Tail Incidence	i_w, i_t	2 deg	Estimated
Fuselage Cross Sectional Areas	S	Varies	Measured
Fuselage Upper Coordinates	Z_U	Varies	Measured
Fuselage Lower Coordinates	Z_L	Varies	Measured

** The propeller modeling software was developed and provided by Jon Becker of Cloud Cap Technologies

The inputs to Digital Datcom were visualized in Tecplot, Fig. (6), prior to running the stability and control analysis. This extra step ensured the measurements resulted in a properly configured aircraft. The Rascal's landing gear was represented by making the cross sectional area at the landing gear location slightly larger.

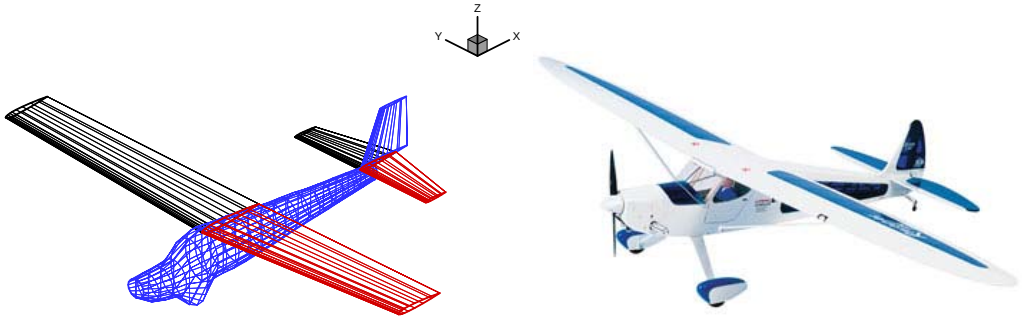

Figure 6. Tecplot Representation of Rascal 110 Model and Actual Rascal 110

H. Datcom Outputs – Stability Derivatives

Datcom outputs a significant amount of useful data. Not all will be used or presented here. The major components of the coefficients of Lift, Drag, and Moment are listed in Table (11). Stability Derivatives are listed in Table (12).

Table 11. Component Lift, Drag, and Moment Coefficients

Coefficient	Symbol	Value	Datcom Output Line #
Wing Coefficient of Lift at 0° AoA	C_{Lo_w}	.421	277
Wing Coefficient of Lift per AoA	$C_{L\alpha_w}$	4.59	276-277
Wing Minimum Coefficient of Drag	$C_{D\min_w}$	0.011	274 at AoA = -6°
Wing Moment Coefficient	C_{M_w}	-0.005	277 at AoA = 0°
Vert. Tail Coefficient of Lift per AoA	$C_{L\alpha_t}$	0.0969	190
Vert. Tail Minimum Coefficient of Drag	$C_{D\min_t}$	0.001	409 at AoA = -10°
Horiz. Tail Coefficient of Lift per AoA	$C_{L\alpha_h}$	0.76	346
Horiz. Tail Minimum Coefficient of Drag	$C_{D\min_h}$	0.002	345 at AoA = -2°
Fuselage Moment Coefficient per AoA	$C_{M\alpha_f}$	0.114	209 at AoA = 0°
Fuselage Coefficient of Drag	C_{D_f}	0.005	209 at AoA = 0°

Table 12. Rascal Stability Derivatives at Trimmed Steady Level Flight Sea Level, Mach = 0.061

Lateral	Value per degree	Lateral	Value per degree	Longitudinal	Value per degree
C_{l_r}	0.01	C_{y_β}	-0.0056	C_{L_α}	0.11
C_{n_r}	-0.0006	C_{l_β}	-0.0018	C_{m_α}	-0.006
$C_{l_{\delta a}}$	0.244	C_{n_β}	0.00023	C_{m_q}	-0.233
$C_{n_{\delta a}}$	-0.0128	C_{l_p}	-0.013	$C_{m_{\delta e}}$	0.011

I. Hardware in the Loop Aircraft Model Inputs

Nearly all the inputs to the Datcom analysis model were also input to the HITL Model. The HITL model considered additional parameters not entered into Datcom. Developed by Cloud Cap Technologies, an outline and sample aircraft model were included with the HITL.[12] Rascal specific parameters for the wing, horizontal and vertical tail surfaces, fuselage, propeller, engine, weights, Inertia, and Airfoil were input. Additional information included the aircraft contact points, sensor, and actuator data. The default aircraft sensor and actuator data provided by Ref. 12 were used.

J. Modeling Errors

Since the exact aircraft was not modeled, errors are introduced as assumptions and conversions are made. By using the E193 airfoil for the simulation, a slightly more conservative estimate of the aerodynamic performance is introduced. When the E193 was converted to a NACA 4310 for Digital Datcom, some rounding was required to fit the E193 to the NACA system of designation. Calculations of the AR used the method for non-rectangular wings and resulted in a 12% increase compared to the method for a rectangular wing. The engine model in the HITL simulation was a linear assumption, although most engines have a non-linear power curve. The landing gear was not modeled directly, but rather incorporated into the fuselage for Digital Datcom.

IV. Simulation

The first simulation was developed in a Matlab/SIMULINK environment and includes the component build up of force, moment, and state equations. An explanation about the set up and use of the HITL simulation is second.

A. Matlab/SIMULINK Simulation

In Matlab, the aerodynamic math model developed in Section III was input, along with equations for the aircraft's forces and moments. These forces and moments were later used to find the trimmed, or steady level flight condition of the simulator at prescribed airspeed settings. The forces, moments, and the 12 initial steady level flight conditions became inputs to a SIMULINK build up to evaluate the model over time. The SIMULINK program calls upon another set of files to calculate the 12 equations of motion of the aircraft. The output of the SIMULINK simulation is then evaluated in response to throttle, elevator, aileron, and rudder input commands

The Matlab simulation began by entering components of the model developed in Section III. In addition to the inputs from Section III, the flight conditions of the simulation required defining. Simulation airspeeds ranged from 64 – 90 feet per second to match the variation in airspeeds encountered during actual flight test. The other simulation flight parameters are density and gravity at 1100 feet above sea level.

B. Forces and Moments Build Up

The basic forces and moments that act upon an aircraft are listed below. The forces of Lift (*L*), Drag (*D*), and Sideforce (*Y*) act in the z, x, and y-axis respectively. The Roll (*l*), Pitch (*m*), and Yaw (*n*) moments, act about the x, y, and z-axis respectively. Reference 10 illustrates the moments and the axis about which they act, see Fig. (7).

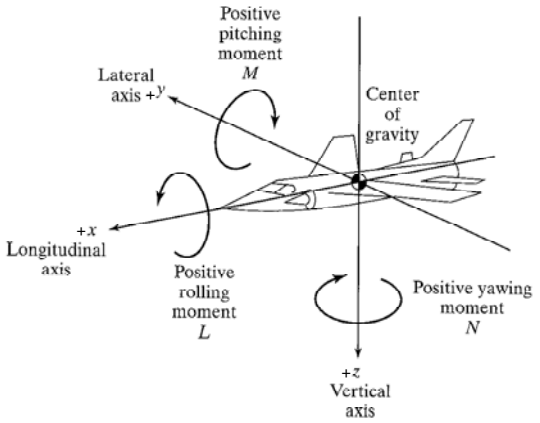

Figure 7. Aircraft Moments; Axis and Direction Definitions[10]

Each of the general force and moment equations listed below can be found in nearly all aerodynamics and control texts. Force and moment equations share the similar components of dynamic pressure ($\bar{q}$), wing reference area (***S***), wing span (***b***), and reference chord length ($\bar{c}$). However, the coefficient (***C***) build up is unique, and is discussed next.[13]

$$L = \bar{q}SC_L \tag{10}$$

$$D = \bar{q}SC_D \tag{11}$$

$$Y = \bar{q}SC_y \tag{12}$$

$$l = \bar{q}SbC_l \tag{13}$$

$$m = \bar{q}S\bar{c}C_m \tag{14}$$

$$n = \bar{q}SbC_n \tag{15}$$

Where,

$$\bar{q} = 0.5\rho V^2 \tag{16}$$

The coefficients that contribute to each of the forces and moments are constructed by the surface they act upon. All the aerodynamic coefficients acting upon the wing are collected in separate equations (14). The horizontal tail, fuselage, and vertical tail are also collected respectively. This notation and collection of terms is derived from Refs. 14 and 15.

$$C_{L_w} = C_{L_{ow}} + C_{L_{aw}}\alpha \tag{17}$$

$$C_{D_w} = C_{D_{\min w}} + K_w C_{L_w}{}^2 \tag{18}$$

$$E = 2\left(C_{L_{ow}} + C_{L_{aw}}\left(\alpha - \dot{\alpha}\frac{\left(cg_t + cg_w\right)}{V} \right) \right) / \left(\pi AR_w\right) \tag{19}$$

$$\alpha_t = \alpha + i_t + T_e d_e + q\frac{cg_t}{V} - E \tag{20}$$

$$C_{L_t} = C_{L_{at}}\alpha_t \tag{21}$$

$$C_{D_t} = C_{D_{\min t}} + K_t C_{L_t}{}^2 \tag{22}$$

$$C_{m_f} = C_{m_{af}}\alpha \tag{23}$$

$$C_{D_{vt}} = C_{D_{\min vt}} \tag{24}$$

$$C_{lp} = -\frac{1}{12} C_{L_{aw}} \frac{(1+3\lambda)}{(1+\lambda)} \tag{25}$$

The forces and moments are now re-written with respect to wing, tail, fuselage, and vertical tail. Eqs. (15).

$$L_W = \bar{q} S C_{L_W} \tag{26}$$

$$D_w = \bar{q} S C_{D_w} \tag{27}$$

$$M_w = \bar{q} S c C_{m_w} \tag{28}$$

$$L_t = n_t \bar{q} S_t C_{L_t} \tag{29}$$

$$D_t = n_t \bar{q} S_t C_{D_t} \tag{30}$$

$$D_f = \bar{q} S c C_{m_f} \tag{31}$$

$$M_f = \bar{q} S c C_{m_f} \tag{32}$$

$$D_{vt} = n_t \bar{q} S_{vt} C_{D_{vt}} \tag{33}$$

Figures (8) and (9) illustrate the component forces and moments above in for the wing only and the wing and tail together respectively.[14]

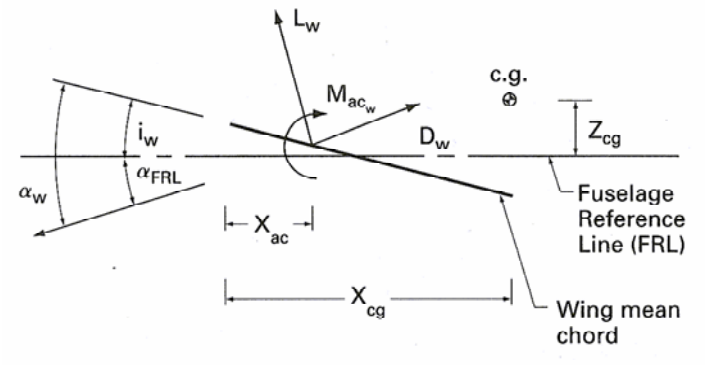

Figure 8. Wing Forces and Moments[14]

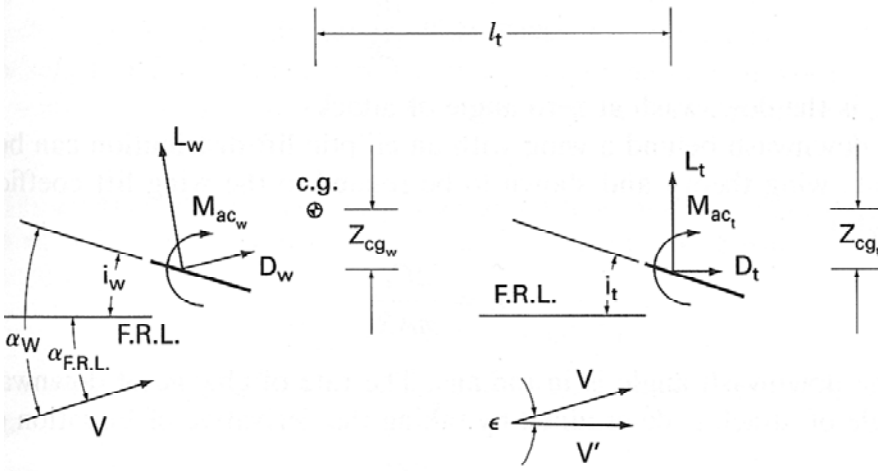

Figure 9. Wing and Tail Forces and Moments[14]

The final force and moment equations (34-39) used for simulation are presented below.[14,15]

$$L = L_w + L_t \cos\left(E - \frac{qcg_t}{V}\right) - \left(D_t + D_{vt}\right)\sin\left(E - \frac{qcg_t}{V}\right) \tag{34}$$

$$D = D_w + \left(D_t + D_{vt}\right)\cos\left(E - \frac{qcg_t}{V}\right) + L_t \sin\left(E - \frac{qcg_t}{V}\right) + D_f \tag{35}$$

$$Y = n_{vt} q_b S_{vt} C_{L_{avt}} \left(-\beta + T_r d_{rt} + \frac{rcg_t}{V}\right) \tag{36}$$

$$\begin{aligned} m = {} & L_w cg_w \cos(\alpha) + D_w cg_w \sin(\alpha) + M_w - L_t cg_t \cos\left(\alpha - E + \frac{qcg_t}{V}\right) \\ & -\left(D_t + D_{vt}\right) cg_t \sin\left(\alpha - E + \frac{qcg_t}{V}\right) + M_f \end{aligned} \tag{37}$$

$$n = -q_b n_{vt} S_{vt} C_{L_{avt}} \left(-\beta + T_r d_{rt} + \frac{rcgt}{V}\right) cg_{vt} + \left(-q_b SbC_{nda} d_a\right) \tag{38}$$

$$l = \frac{q_b Sb^2}{2V}\left(C_{lp} p + \frac{2V}{b} C_{lb}\beta + C_{lr} d_{rt} + \frac{C_{lda} d_a 2V}{b}\right) \tag{39}$$

C. Equations of Motion

The best equations to completely and accurately model an aircrafts true motion are non-linear ordinary differential equations.[16] Various simplifications of the equations listed above can be used, however, "the most accurate dynamic model for a full envelope flight simulation is one based on the nonlinear fully coupled equations of motion."[16] Despite the robust nature of these nonlinear fully coupled equations of motion, they are also the most complex to handle. Due to the nature of these nonlinearities, no closed form solution exists, and numerical methods must be used to solve for a steady state solution.[16]

Aircraft move with six degrees of freedom along three axis.[10] Motion caused by gravity, propulsion, and aerodynamic forces contribute to the forces and moments that act upon the body.[13] To begin, makes several major assumptions are made.[15] First, the aircraft is rigid.[13] Although aircraft are truly elastic in nature,[13] modeling the

flexibility of the UAV will not contribute significantly to the research at hand. Second, the earth is an inertial reference frame.[13] Third, aircraft mass properties are constant through out the simulation.[13] Finally, the aircraft has a plane of symmetry.[13] The first and third assumptions allow for the treatment of the aircraft as a point mass. Table (13) defines each of the variables used in the Equations of Motion.[13]

Table 13. Flight Path Components Variable Definition

Flight Path Components	
Variable	**Symbol**
Roll Rate (rad/sec)	P
Pitch Rate (rad/sec)	Q
Yaw Rate (rad/sec)	R
Velocity (ft/sec)	V
Sideslip Angle (rad)	β
Angle of Attack (rad)	α
Bank Angle (about velocity vector, in rads)	μ
Flight-Path Angle (rad)	γ
Heading Angle (rad)	χ
North Position (ft)	ξ
East Position (ft)	η
Altitude (ft)	h

V, χ, and γ represent the magnitude of the velocity vector, heading angle, and flight path angle respectively.[13] P, Q, and R represent the components of angular velocity; roll, pitch, and yaw, respectively.[13] The position of the aircraft relative to the earth in Cartesian coordinates is ξ, η, and h.[13] Body attitude relative to the velocity vector are μ, β, and α.[15] The 12 six-degree of freedom, nonlinear, and fully coupled ordinary differential equations of motions assume that lift is perpendicular and drag is parallel to inertial velocity, Eqs. (41-52).[13]

$$I_{xx}\dot{p} - I_{xz}\dot{r} = l + I_{yy}rq + I_{xz}pq - I_{zz}qr \tag{41}$$

$$I_{yy}\dot{q} = m - I_{xz}p^2 + I_{zz}pr - I_{xx}rp + I_{xz}r^2 \tag{42}$$

$$-I_{xz}\dot{p} + I_{zz}\dot{r} = n + I_{xx}pq - I_{xz}qr - I_{yy}pq \tag{43}$$

$$\dot{V} = \frac{1}{m}\left(-D\cos\beta + Y\sin\beta + T\cos\beta\cos\alpha\right) - g\sin\gamma \tag{44}$$

$$\dot{\chi} = \frac{1}{mV\cos\gamma}\left[D\sin\beta\cos\mu + Y\cos\mu\cos\beta + L\sin\mu + T\left(\sin\mu\sin\alpha - \cos\mu\sin\beta\cos\alpha\right)\right] \tag{45}$$

$$\dot{\gamma} = \frac{1}{mV}\left[-D\sin\beta\sin\mu - Y\sin\mu\cos\beta + L\cos\mu + T\left(\cos\mu\sin\alpha + \sin\mu\sin\beta\cos\alpha\right)\right] - \frac{g\cos\gamma}{V} \tag{46}$$

$$\dot{\mu} = \frac{p\cos\alpha + r\sin\alpha}{\cos\beta} + \frac{1}{mV}\begin{bmatrix} D\sin\beta\cos\mu\tan\gamma + Y\tan\gamma\cos\mu\cos\beta + L\left(\tan\beta + \tan\gamma\sin\mu\right) \\ +T\left(\sin\alpha\tan\gamma\sin\mu + \sin\alpha\tan\beta - \cos\alpha\tan\gamma\cos\mu\sin\beta\right) \end{bmatrix} - \frac{g\cos\gamma\cos\mu\tan\beta}{V} \tag{47}$$

$$\dot{\alpha} = q - \tan\beta\left(p\cos\alpha + r\sin\alpha\right) - \frac{1}{mV\cos\beta}\left(L + T\sin\alpha\right) + \frac{g\cos\gamma\cos\mu}{V\cos\beta} \tag{48}$$

$$\dot{\beta} = -r\cos\alpha + p\sin\alpha + \frac{1}{mV}\left(D\sin\beta + Y\cos\beta - T\sin\beta\cos\alpha\right) + \frac{g\cos\gamma\sin\mu}{V} \tag{49}$$

$$\dot{\xi} = V\cos\gamma\cos\chi \tag{50}$$

$$\dot{\eta} = V\cos\gamma\sin\chi \tag{51}$$

$$\dot{h} = V\sin\gamma \tag{52}$$

D. SIMULINK

The SIMULINK model was designed to accept the exact same control surface inputs sent to the flight test vehicle, and use the math model to determine the response. For the first 100 seconds the SIMULINK simulation is running, only trim conditions are sent to the control surfaces. The trim condition was established by achieving steady, level, unaccelerated flight. Table (14) lists the trim conditions at a true airspeed of 64.8 feet per second input to SIMULINK for the first 100 seconds. The trim condition is confirmed by examining the output altitude, and the pitch, roll, and yaw rates.

Table 14. Example Trim Conditions for Given Velocity and Altitude

At given Velocity	64.8280 ft/sec
At given Altitude	1119 ft MSL
Throttle Trim	1.29
Elevator Trim	- 0.1174 rads
Rudder Trim	0 rads
Aileron Trim	0 rads
AoA Trim	-0.0153 rads

The trim conditions are sent as inputs, labeled steady level flight/Trim Conditions on the SIMULINK diagram. At 100 seconds, a commanded deflection is sent to one of the control surfaces. The commanded deflection is taken from the telemetry data collected during flight test, ensuring the commands are identical. The trim conditions, in addition to other initial conditions make up the initial state vector used to begin solving the 12 non-linear differential equations of motion introduced above. The initial state vector with the trim conditions is listed in Table (15).

Table 15. Equations of Motion Initial Conditions for Trimmed Flight at Given Velocity and Altitude

State	Trim Value
P	0 rads/sec
Q	0 rads/sec
R	0 rads/sec
V	64.8280 ft/sec
β	0 rads
α	-0.0153 rads
μ	0
γ	0
χ	0
ξ	0
η	0
h	1119 ft MSL

The SIMULINK diagram below, Fig. (10), shows the complete simulation set up. The control inputs and trim conditions are input from the left and plotted on a scope for verification. Then the equations of motion are called. The outputs from the equations of motion are integrated prior to plotting.

The SIMULINK Elevator input command (de) and Altitude output response (h) are presented, Fig. (11). The throttle and elevator setting are held the previously mentioned constant values required for trimmed flight. The ailerons and rudder are held at zero deflection since no lateral inputs are required for steady level flight. At 100 seconds, the input to the elevator is commanded and then returns to its trimmed setting and the aircraft is allowed to oscillate in response.

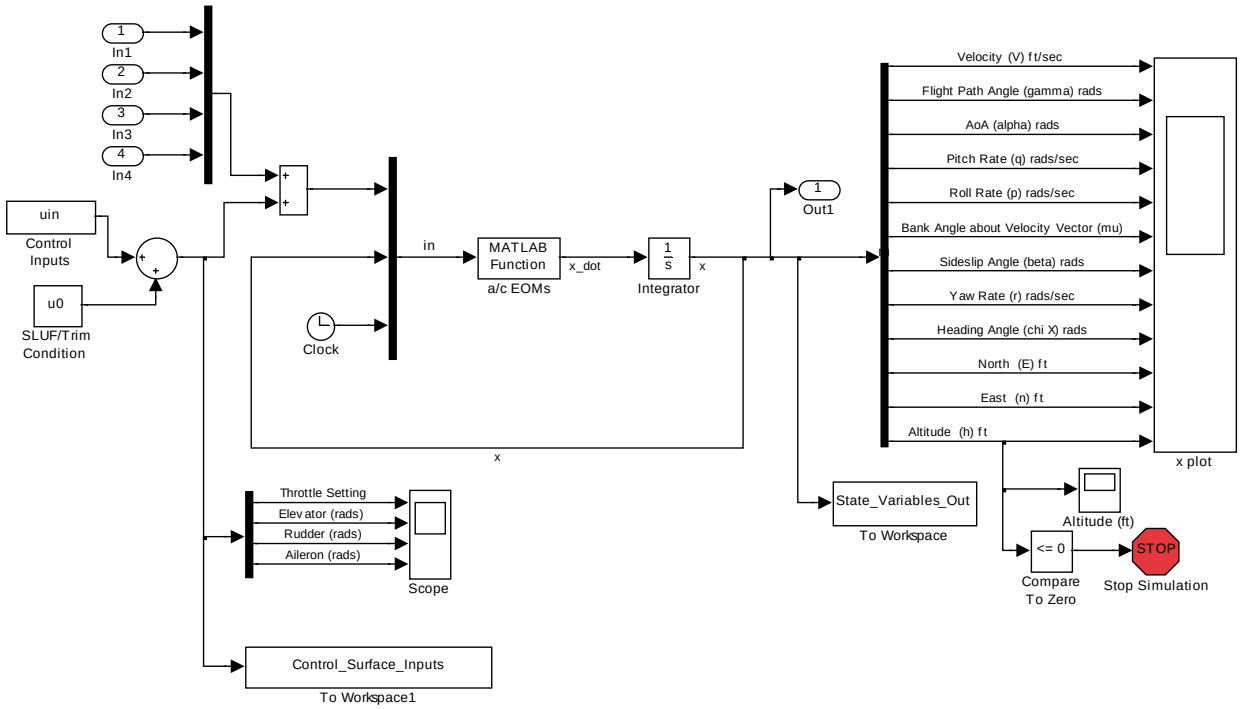

Figure 10. SIMULINK UAV Simulation

The altitude response, second plot in Fig. (11), is of primary interest, as it is used for analysis of the aircraft's longitudinal response. Notice the aircraft is flying level prior to the elevator deflection. All 12 states of the simulation are output for the duration of the 300 second run. All aircraft states are constant until the elevator input. Only the north position vector shows an increase in distance flown, but no deviation to the east, indicating a straight flight path in a northerly heading. Only pitch rate, angle of attack, velocity, flight path angle, and altitude change with respect to the elevator inputs. Roll rate, bank angle, sideslip, yaw rate, and heading angle all remain unchanged with respect to the elevator inputs. All the results are expected for the input command; preliminary indications the simulation is functioning properly.

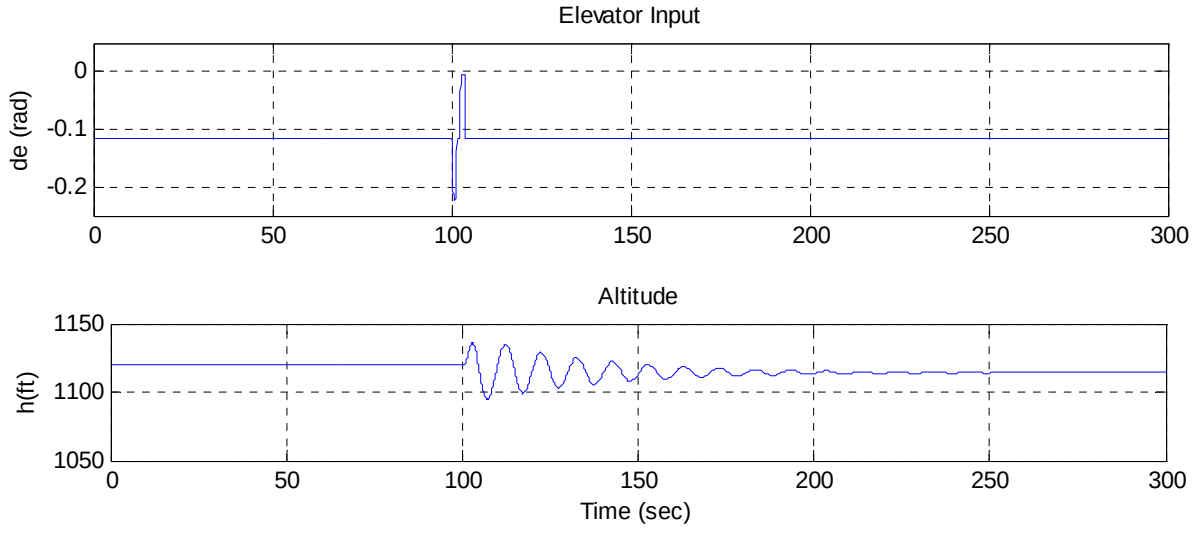

Figure 11. SIMULINK Simulation Elevator Input and Altitude Output

E. Hardware in the Loop Simulation

The HITL simulation, provided by Cloud Cap Technologies,[12] was used extensively for laboratory flight simulation and test team training. The HITL simulation used the same Operator Interface used during flight. The HITL environment is very nearly representative of the airspace and flight conditions of the Rascal although several differences exist though. The wind conditions experienced in the test flights were not reproduced. No wind conditions were desired for simulation, and a majority of flight tests were conducted on calm days. Altitude and airspace restrictions were not observed during flight in the HITL simulation. This would over constrain the simulation, and minimize its usefulness.

The HITL simulation uses the model constructed in Section III. The gain settings, waypoints, and all other parameters input to the Operator Interface were also identical to the settings input during actual flight.

V. Flight Test of UAV Platform

Section V details the flight-testing introduced in Section II. The procedures and maneuvers flown for both open loop airframe and autonomous flight tests. Also discussed are flight-test issues encountered during the research.

A. Open Loop Flight Tests

The challenge of implementing the procedures for open loop flight test required overcoming significant testing issues such as weather, equipment, scheduling, and ambiguities in aircraft attitudes. Development of a flight-test plan structured and maximized flight time. Each flight establishment of a constant communications link with the aircraft in order to collect telemetry at 20 Hz. Maneuvers were flown either into the wind or with the wind. Cross wind maneuvers were not flown.

B. Flight Procedures and Configurations

The procedures for executing each maneuver were carefully scripted ahead of time. After take off, the pilot flew the aircraft to the end of the airspace and aligned it with the runway. The aircraft flew at airspeeds between 60 and 90 feet per second, as determined by the maneuver to be performed. Test altitudes were 1100 feet. The pilot then established a trimmed and steady level flight condition. A log of each maneuver was maintained, noting the start and end time, and corresponded Operator Interface clock in the telemetry log file.

C. Maneuvers

The pilot performed the phugoid and short period pitch maneuvers.[17] Only the elevator was used to perform the maneuver, while the throttle, ailerons, and rudder were held in trim position. The phugoid maneuvers were started from trimmed flight when the pilot input a nose up command to bleed airspeed. Several practice runs were performed to determine the correct pitch up angle to bleed about 15 feet per second of airspeed. Telemetry read outs from the Operator Interface determined the changes in airspeeds. Once the pitch up maneuver was performed, the pilot returned the elevator to the trimmed position and allowed the aircraft to oscillate until all the oscillations damped out.[17]

The short period maneuver was performed in much the same way as the phugoid. Where the phugoid was just a nose up maneuver, the short period is a nose up, nose down, and back to trim procedure. Again, just the elevator was used and all maneuvers began from steady level flight.

VI. Results

The results of open loop flight tests are compared against the simulations. Additionally, the Matlab/SIMULINK simulation is compared against the Hardware in the Loop (HITL) simulation. Only longitudinal maneuvers were performed. Varied elevator commands sought to excite the phugoid and short period modes of the aircraft.

In Fig. (12), the aircraft was trimmed at 64 feet per second when the elevator doublet command was input. The aircraft exhibited 30 feet higher altitude gains than the Matlab simulation during the initial oscillation. The period of oscillation was longer in flight as compared to the simulation's output. The input commands to both simulators were identical. The altitude plot also reveals the aircraft was in a slight climb prior to the input, suggesting it was not in true steady level unacceleratied flight. This is confirmed by the True Airspeed (TAS) plot, which shows decreasing airspeed prior to the commanded input. The aircraft also has a higher pitch rate than the Matlab/SIMULINK simulation. Airspace limitations prevented the aircraft oscillations from damping out entirely before the pilot had to turn back.

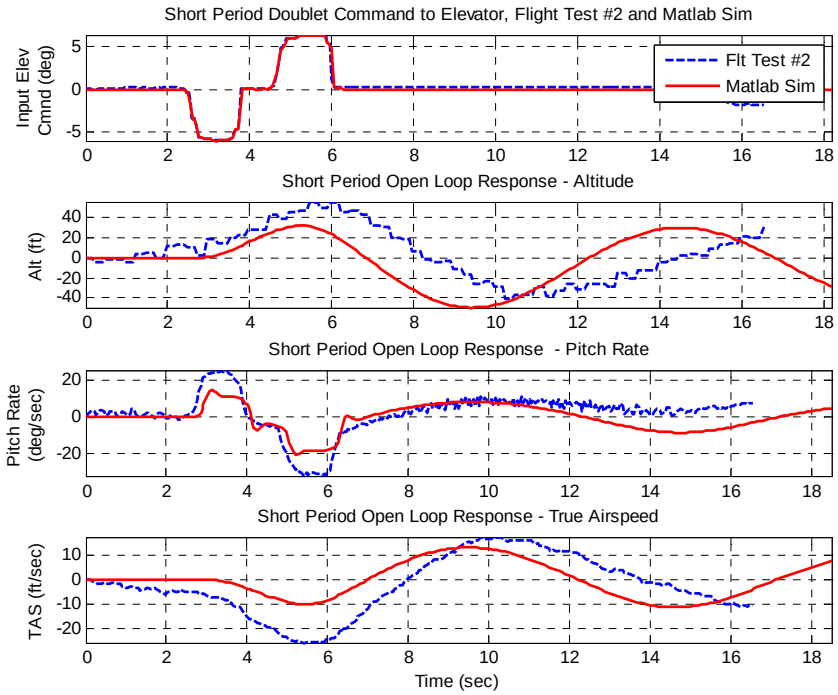

Figure 12. Short Period Response to Elevator Doublet – Flight Test #2 v Matlab Sim

The Hardware in the Loop simulation tended to match the Matlab simulation better than the flight test comparisons, Fig. (13). The initial periods line up, but the oscillations quickly fall out of phase with each other, indicating the pitch damping of the HITL simulation is slightly higher than the Matlab simulation. Overall, the response to the elevator input shows positive results. They tend to damp out at roughly the same rate and nearly reach the same amplitudes.

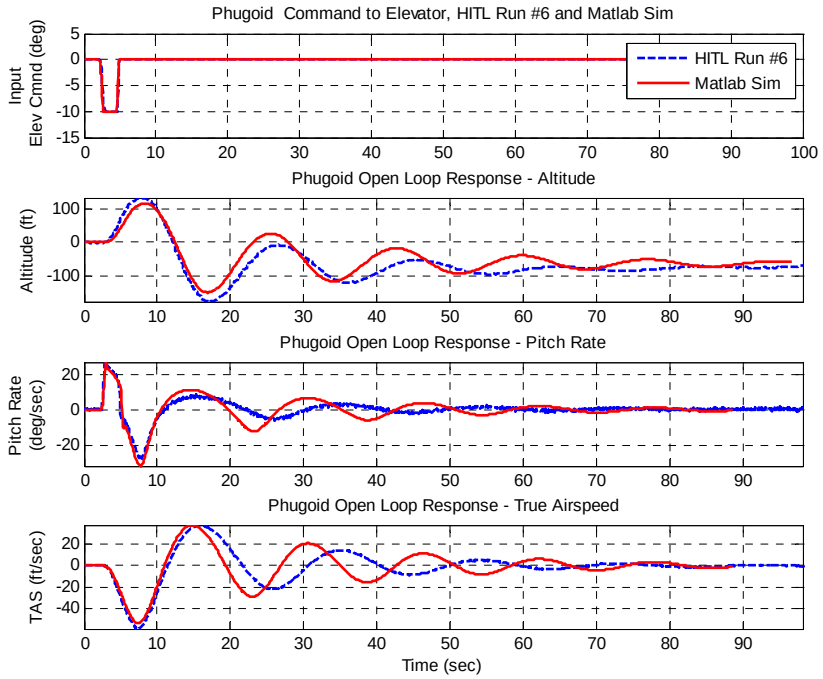

Figure 13. Comparison of HITL Run #6 to Matlab Sim; Elevator Input

Figure (14), represents the results of another HITL and Matlab comparison. The input here is much smaller than the previous comparison. The response is similar to the previous in terms of damping and oscillations. As expected, altitude was not as high, due to the smaller input. This output was expected and shown.

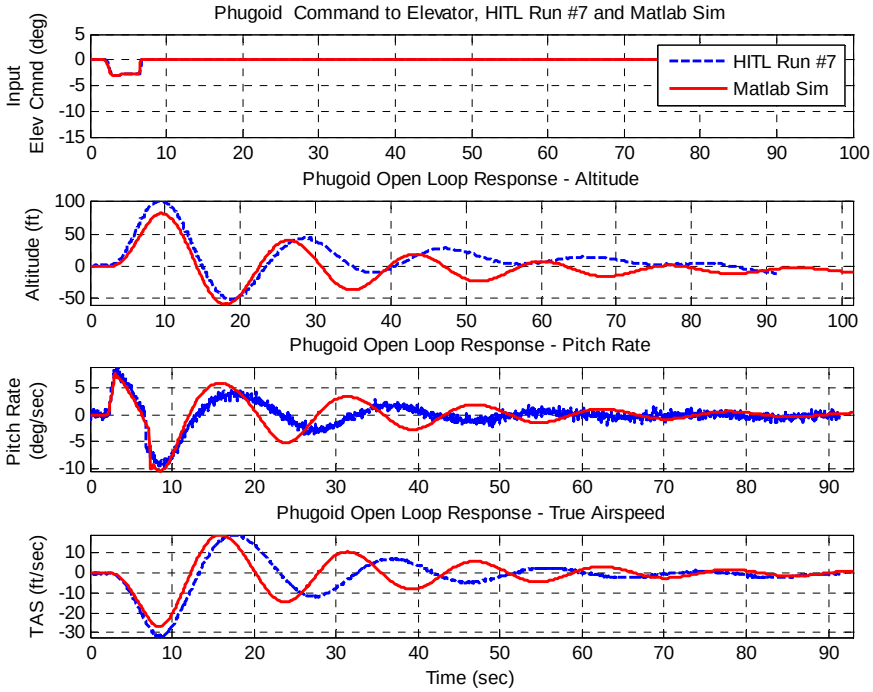

Figure 14. Comparison of HITL Run #7 to Matlab Sim; Elevator Input

VII. Conclusions

The research developed a straightforward procedure for producing a physical, inertial, and aerodynamic model for small Unmanned Aerial Vehicle. The model was then incorporated into a six degree of freedom Matlab/SIMULINK and Hardware in the Loop Simulation. Open loop flight test revealed the dynamic flying qualities of the aircraft. This data validated the simulation model, and highlighted areas for improvement, such as increasing the pitch damping of the simulation. Additionally, both Hardware in the Loop and Matlab/SIMULINK simulations tended to have less damped oscillations as compared to the flight test results.

Flight test results were positive overall. The process of fly, analyze in Matlab, Hardware in the Loop simulate, and fly again proved invaluable.

Future simulations could incorporate wind tunnel tests of the aircraft. In turn, Digital Datcom output could be compared to wind tunnel results. A dynamometer bench test of the engine would produce an improved model. Mapping the RPM's, torque, and power will allow the simulation to run a variety of power settings.

The views expressed in this article are those of the author and do not reflect the official policy or position of the United States Air Force, Department of Defense, or the U.S. Government.

Appendix

Table 16. Available Telemetry from Piccolo II Autopilot Logs

1. System Time in milliseconds (From power up of Operator Interface and Ground Station)
2. Current Day, Month, Year, Hours, Minutes, and Seconds from GPS
3. Latitude and Longitude (rads)
4. GPS Height above Sea Level (m)
5. GPS Ground Speed and Pitot Static Airspeed (m/s)
6. Various Autopilot, Servo, and Battery Health Status parameters
7. Barometric Altitude above sea level (m)
8. Static and Dynamic Pressures (Pa)
9. Pitch, Roll, and Yaw Rates (rads/sec)
10. X, Y, and Z Axis Accelerations (m/s/s)
11. Pitch, Roll, and Yaw Angles (rads)
12. Throttle Position (1 = Full Throttle, 0 = Cut Off)
13. Elevator, Aileron, and Rudder Positions (rads)
14. Autopilot Command Status (On/Off)
15. Current Altitude, Turn, Waypoint, Airspeed, and Flap Setting Commands

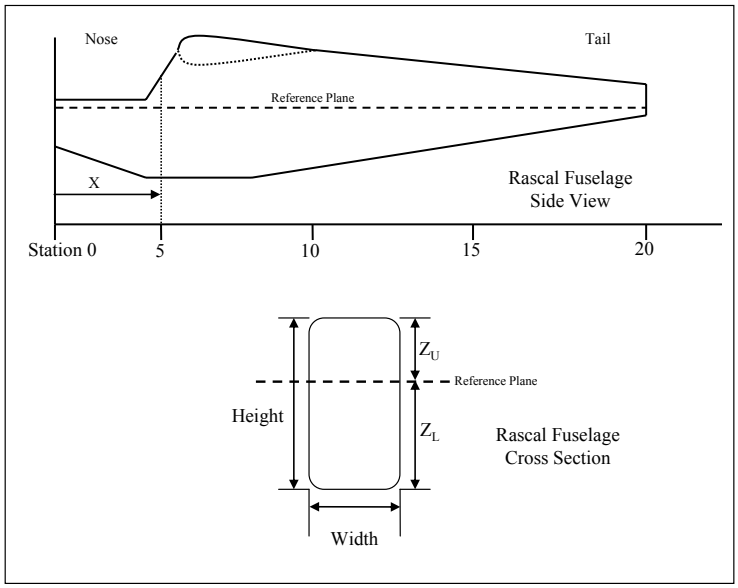

Figure 15. Definitions of Fuselage Cross Sectional Measurements

Table 17. Rascal 110 Fuselage Cross-Sectional Measurements

Station	*X (ft)*	*S (ft^2)*	*Z_U (ft)*	*Z_L (ft)*
0	0.000	0.104	0.009	0.167
1	0.292	0.195	0.016	0.354
2	0.583	0.245	0.020	0.438
3	0.875	0.285	0.024	0.479
4	1.250	0.573	0.048	0.813
5	1.542	0.458	0.038	0.479
6	1.750	0.439	0.037	0.458
7	2.042	0.420	0.035	0.458
8	2.333	0.401	0.033	0.438
9	2.625	0.352	0.029	0.417
10	2.917	0.313	0.026	0.396
11	3.208	0.272	0.023	0.375
12	3.500	0.234	0.020	0.333
13	3.792	0.194	0.016	0.313
14	4.083	0.152	0.013	0.292
15	4.375	0.120	0.010	0.271
16	4.667	0.087	0.007	0.250
17	4.958	0.063	0.005	0.229
18	5.250	0.042	0.003	0.208
19	5.542	0.024	0.002	0.188

Table 18. E193 Airfoil Data at Re = 204,200

alpha	*CL*	*Cdo*	*Cdi*	*CD*
-3.94	-0.106	0.0148	0.0006	0.0154
-2.95	-0.017	0.0129	2E-05	0.0129
-1.89	0.085	0.0123	0.0004	0.0127
-0.88	0.179	0.0106	0.0017	0.0123
0.15	0.298	0.01	0.0047	0.0147
1.18	0.401	0.0107	0.0086	0.0193
2.19	0.505	0.0112	0.0136	0.0248
3.22	0.608	0.0122	0.0197	0.0319
4.24	0.706	0.0127	0.0266	0.0393
5.26	0.803	0.0134	0.0344	0.0478
6.28	0.898	0.0133	0.043	0.0563
7.31	0.98	0.0147	0.0513	0.066
8.31	1.04	0.0177	0.0577	0.0754
9.31	1.081	0.0221	0.0624	0.0845
10.33	1.103	0.0282	0.0649	0.0931
11.34	1.104	0.0326	0.0651	0.0977
12.33	1.1	0.0382	0.0646	0.1028

References

[0]Jodeh, N., *Development of Autonomous Unmanned Aerial Vehicle Research Platform: Modeling, Simulating, and Flight Testing,* MS Thesis, AFIT/GAE/ENY/06-M18, School of Engineering and Management, Air Force Institute of Technology (AU), Wright-Patterson AFB, OH, March 2006.

[1]Ly, L. and Higashino, S. "Development of a UAV-Flight Test Vehicle at the University of Washington," *Presented at the 2nd AIAA "Unmanned Unlimited" Systems, Technologies, and Operations – Aerospace Conference,* 15-18 September 2003.

[2]King, E., *Distributed Coordination and Control Experiments on a Multi-UAV Testbed,* MS Thesis, Department of Aeronautics and Astronautics, Massachusetts Institute of Technology, MA, September 2004.

[3]Johnson, E., and Fontaine, S., "Use of Flight Simulation to Complement Flight Testing of Low-Cost UAVs," School of Aerospace Engineering, Georgia Institute of Technology, American Institute of Aeronautics and Astronautics, 2001, (AIAA 2001-4059).

[4]Foster, T., and Bowman, J., "Dynamic Stability and Handling Qualities of Small Unmanned-Aerial-Vehicles," *43rd AIAA Aerospace Sciences Meeting and Exhibit,* January 2005, (AIAA 2005-1023).

[5]Higgs, Travis J. *Modeling, Stability, and Control of a RotaTable Tail on a Micro Air Vehicle,* MS Thesis, AFIT/GAE/ENY/06-D05, School of Engineering and Management, Air Force Institute of Technology (AU), Wright-Patterson AFB, OH, March 2006.

[6]Frew, E., Xiao, X., Spry, S., McGee, T., Kim, Z., Tisdale, J., Sengupta, R., Hendrick, K.J., "Flight Demonstrations of Self-directed Collaborative Navigation of Small Unmanned Aircraft," *Proceedings of the 2004 IEEE Aerospace Conference*, Big Sky, MT, March 2004.

[7]Office of the Sectretary of Defense, *Unmanned Aerial Vehicles Roadmap 2002-2027,* Washington: HQ DOD, December, 2002.

[8]*SIG Rascal 110 ARF Assembly Manual,* SIG Manufacturing Company, Inc., Montezuma, IA.

[9]Miller, M.P. An Accurate Method of Measuring the Moments of Inertia of Airplanes, *Technical Notes: National Advisory Committee for Aeronautics,* Washington DC, Langly Memorial Aeronautical Laboratory, #351, October, 1930.

[10]Bertin, J., *Aerodynamics for Engineers,* 4th ed., Upper Saddle River, New Jersey. Prentice-Hall, 2002.

[11]Hoak, D.E, Ellison, D.E., et al., "USAF Stability and Control Datcom," Unpublished, AF Flight Dynamics Laboratroy AFFDL-TR-79-3032, April 1979

[12]Vaglienti, B., Niculescu, M., *Hardware in the Loop Simulator for the Piccolo Avionics,* Hood River, OR, Cloud Cap Technology, 18 April 2005.

[13]Honeywell Technology Center, "Application of Multivariable Control Theory to Aircraft Control Laws: Final Report, March 1993 – March 1996," Contract f33615-92-C-3607, Paper *WL-TR-96-3099,* Minneapolis, MN., May 1996 (ADA315259).

[14]Nelson, R. C., *Flight Stability and Automatic Control* (Second Edition), Madison, WI, McRaw-Hill, 1998.

[15]Enns, D., AEM 5319: Dynamics, Stability, and Control of Aerospace Vehicles, University of Minnesota, May, 1994, (unpublished class notes).

[16]Sadraey, M., and Colgren, R., "UAV Flight Simulation: Credibility of Linear Decoupled vs. Nonlinear Coupled Equations of Motion," *AIAA Modeling and Simulation Technologies Conference and Exhibit,* August, 2005, (AIAA 2005-6425).

[17]Kimberlin, Ralph D., *Flight Testing of Fixed Wing Aircraft,* Reston, VA, American Institute of Aeronautics and Astronautics, 2003

Etkin, B. and Reid, L.D., *Dynamics of Flight, Stability and Control,* 3rd ed, New York, NY., John Wiley and Sons, Inc., 1996.

Roskam, J., *Airplane Flight Dynamics and Automatic Controls*, Ottawa, KS, Roskam Aviation and Engineering Corporation, 1979.